ACS APPLIED MATERIALS & INTERFACES

Research Article

www.acsami.org

Au/Au@Polythiophene Core/Shell Nanospheres for Heterogeneous Catalysis of Nitroarenes

Hye-Seon Shin and Seong Huh*

Department of Chemistry and Protein Research Center for Bio-Industry, Hankuk University of Foreign Studies, Yongin 449-791, Korea

Supporting Information

ABSTRACT: Monodisperse Au/Au@polythiophene core/shell nanospheres were facilely prepared through the reduction of gold precursor, $AuCl_4^-$, by 2-thiopheneacetonitrile in an aqueous solution. Concomitantly, 2-thiopheneacetonitrile polymerized during this redox process. As a result, Au nanoparticle was encapsulated by conductive polymer shell to afford novel core/shell nanospheres. Interestingly, the shell was composed of very tiny Au nanoparticles surrounded with thiophene polymers. Thus, the new material is best described as Au/Au@polythiophene core/shell nanospheres. FT-IR spectroscopy revealed that the Au nanoparticles were coordinated by the C≡N groups of the polythiophene shell. Some of the C≡N groups were partially hydrolyzed into COOH groups during the redox process because of the acidic reaction condition. The shell was conductive based on the typical ohmic behavior found in electrical measurement. The Au/Au@polythiophene core/shell nanospheres were found to be very active catalysts for the hydrogenation of various nitroarene compounds into corresponding aminoarene compounds in the presence of $NaBH_4$. Both hydrophilic and hydrophobic nitroarenes were efficiently hydrogenated under mild conditions.

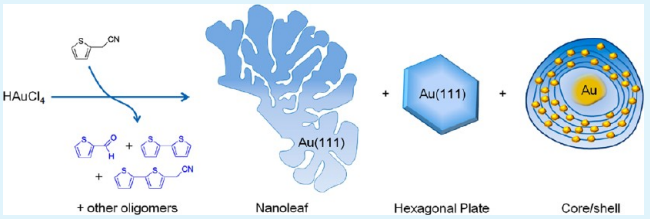

KEYWORDS: *gold nanoparticle, core/shell structure, hydrogenation, nanostructure, Raman spectroscopy*

1. INTRODUCTION

Gold nanoparticles (Au NPs) are key materials in nanochemistry and nanomaterials science. Their excellent particle size- and interparticle distance-dependent optical properties based on surface plasmon resonance (SPR) are useful for a wide range of advanced applications such as colorimetric sensors[1−6] and surface-enhanced Raman scattering (SERS)-based sensory systems.[7,8] Biocompatible Au NPs are also effective delivery carriers for intracellular transport of various cell membrane-impermeable biologically active molecules.[9,10] In addition, there has been growing interest in the catalytic applications of Au NPs since the first report of Au NP-based catalytic system by Haruta et al.[11−13] There is an increasing number of publications on protection of Au NPs in the form of core/shell or yolk/shell type to preserve the active core Au NP. For example, Wu et al. reported Au NP core/shell particles in which the Au NP was encapsulated by hollow mesoporous silica shell.[14] Song et al. also developed yolk/shell type of Au NP system by a controlled etching of Au/silica core/shell NPs.[15] All these materials were active for the catalytic hydrogenation of nitroarene compounds into aminoarenes in the presence of $NaBH_4$ as a hydrogen atom source. One potential drawback of these systems, however, may be the complicated preparation methods with multiple synthetic steps. They usually require silica coating of Au NP which should be prepared separately and subsequent controlled etching of silica shell of Au/silica core/shell to lead to catalytically active target core/shell or yolk/shell type of materials with porous shell. Similarly, Au/C yolk/shell materials were also prepared by Dai et al. through multiple steps.[16]

Our recent report on the preparation of nanogap-rich gold nanoleaf structural motif indicated that the reducing agent, 2-thiophenemethanol, not only reduced the Au(III) precursor but also effectively stabilized the surfaces of the resulting Au nanoleaves.[17] The Au nanoleaf was a very thin nanosheet with abundant nanogaps. The top and bottom surfaces of the Au nanoleaf were exclusively bound with the Au(111) facet as often observed in the triangular Au prisms[18−20] and thin nanoscale Au hexagonal plates.[21,22] The nanogap (∼ 4.8 nm) of Au nanoleaves induced an unusually high enhancement factor (EF) of ∼2×10^8 for the SERS of methylene blue. As a result, a very low concentration of methylene blue solution of 10^{-9} M was detectable. This result raised a new question about the detailed role of other thiophene derivatives with different functionalities at the 2-position of the thiophene ring during the reduction of $AuCl_4^-$ into metallic Au. Hence, we employed another molecule, 2-thiopheneacetonitrile (2-TAN), as a reducing agent for $AuCl_4^-$ in an aqueous solution to exploit the role of 2-thiophene derivatives.

The formal reduction potential of 2-TAN estimated by cyclic voltammetry in the mixed solvent of phosphate buffered saline (PBS, pH 7.0) and acetonitrile (50/50 vol%) was 0.70 V (see

Received: September 10, 2012
Accepted: October 29, 2012
Published: October 29, 2012

   dx.doi.org/10.1021/am3019417 | ACS Appl. Mater. Interfaces 2012, 4, 6324−6331

Scheme 1. Illustration of the Simultaneous Formation of Various Nanoscale Au Structures by 2-TAN

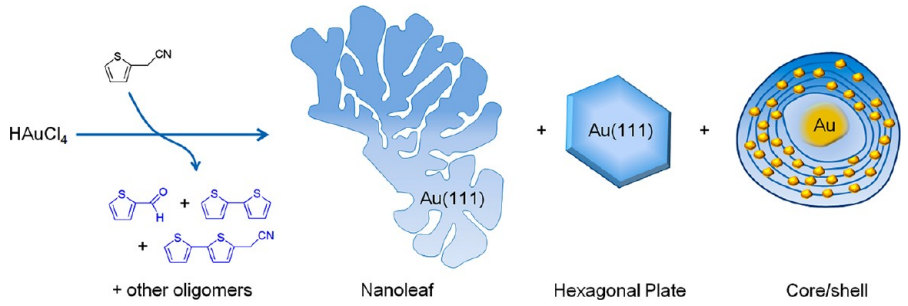

the Supporting Information, Figure S1). This value indicated that $AuCl_4^-$ could be reduced into metallic Au by 2-TAN without the need of other reducing agents. For comparison, the standard reduction potential of $AuCl_4^- + 3e^- \rightarrow Au(s) + 4Cl^-$ is 1.002 V with respect to the standard hydrogen electrode (SHE),[23] and the formal reduction potential of 2-thiophenemethanol in PBS (pH 7.0) is 0.76 V.[8] Here we report on the role of 2-TAN for the reduction of $AuCl_4^-$ and a new type of Au/Au@polythiophene core/shell nanospheres as shown in Scheme 1. These new materials can be prepared by a simple two-step method. This novel core/shell hybrid nanosphere is a very active catalyst for the hydrogenation of various nitroarenes at ambient conditions.

2. EXPERIMENTAL SECTION

Preparation of Au/Au@polythiophene Core/Shell Nanospheres. 2-TAN (22 μL, 0.207 mmol, Aldrich) was added to 10 mL of deionized water and the resulting mixture was vigorously stirred for 1 min. Following this, 0.51 M $HAuCl_4$ aqueous solution (200 μL, Aldrich) was injected into the mixture. The resulting solution was left for 6 h with gentle stirring (70 rpm). The suspended products were collected by centrifugation at 9000 rpm, and the collected precipitates were washed several times with deionized water. The precipitates collected by centrifugation were composed of large Au plates or nanoleaf structures and conducting polymer spheres containing Au core with an average diameter of 30 nm. Pure core/shell nanospheres were obtained by an etching of the as-prepared Au materials by 0.3 M KCN aqueous solution for 30 min. The final Au core/shell nanospheres were centrifuged at 13000 rpm and separated after a few times of washing with deionized water.

Hydrogenation of Nitroarenes. 4-Nitrophenol, 4-nitrotoluene, and nitrobenzene were chosen as substrates for the catalytic hydrogenations in the presence of $NaBH_4$ as a hydrogen source. Each nitroarene solution dissolved in methanol (40 μL, 0.005 M) was added into a quartz cuvette with 2 mL of deionized water and was stirred for 10 min. A freshly prepared aqueous $NaBH_4$ solution (400 μL, 0.05 M) was treated and allowed to stir vigorously for 10 min. Next, the aqueous solution of Au/polythiophene core/shell nanospheres (200 μL, 0.8 mg/mL) was injected under gentle stirring. UV/Vis absorption spectra were recorded with regular intervals to monitor the catalytic reductions of nitroarenes for 2 h.

Physical Measurements. Powder X-ray diffraction patterns were obtained by a Rigaku MiniFlex (30 kV, 15 mA). FE-SEM images and EDS elemental mapping images were recorded on a Hitachi Ultra-High-Resolution Analytical FE-SEM SU-70 (5 kV, magnifications ×10,000 and ×30,000). The water suspension of the sample was dropped and dried on a Cu grid supported by a holey carbon film for TEM measurement, where a JEOL JEM-3000F (300 kV) equipped with an EDAX for EDS spectrum were used. High-angle annular dark field scanning transmission electron microscopy (HAADF-STEM) line scanning analysis was performed on a Tecnai F20 (200 kV) equipped with an EDAX for EDS spectrum. Mass spectrometry was performed on a Thermo Finigan LCQ LC/MS system. XPS data were collected on a K-Alpha X-ray photoelectron spectrometer (Thermo VG, UK). X-ray source was a monochromated Al Kα line ($h\nu$ = 1486.6 eV) and X-ray power was 12 kV and 3 mA. The pass energy of the analyzer for high-resolution spectrum was fixed at 50 eV. Sampling area was 400 μm in diameter. The binding energies were referenced to 284.8 eV (C 1s peak for C−C bonds). The cyclic voltammetry of 2-thiopheneacetonitrile in PBS (phosphate buffered saline, pH 7.0)/CH_3CN (20 mL, 50/50 vol%) was performed using an Ivium CompactStat potentiostat/galvanostat (Ivium Technologies, Netherlands). An Au disc electrode with a dimension of 0.0201 cm^2 was used. A Pt coil and an Ag/AgCl electrode were used as a counter electrode and a reference electrode, respectively. The respective scan rate and scan range were 50 mV/s and 0−1.3 V, respectively. Micro Raman measurements were performed in backscattering geometry with a Horiba Jobin Yvon LabRam HR system fitted with a liquid-nitrogen cooled CCD multichannel detector. The spectra were collected under ambient conditions using either the 514 nm line of an Ar-ion laser or the 633 nm line of a He−Ne laser. Au core/shell nanospheres deposited on Si wafer were exposed with 0.05 mW laser power for 10 s (514 nm) or 30 s (633 nm) of acquisition times with an area of 1 μm.

3. RESULTS AND DISCUSSION

The Au precursor, $AuCl_4^-$, was reduced by 2-TAN in an aqueous solution at room temperature. The as-prepared dark solid products were retrieved from the reaction mixture and analyzed by scanning electron microscopy (SEM). The as-prepared solid materials possessed three different types of Au nanostructures as shown in Scheme 1. Au nanoleaves and Au hexagonal prisms were produced together with monodispersed nanospheres, as depicted in Figure 1a, b. Both Au nanoleaves and Au prisms could be selectively etched away when we used relatively high concentration of KCN etchant (0.3 M KCN) for a short time (30 min). Thus, we were able to obtain pure nanospheres through this process (Figure 1c, d).

The monodisperse nanospheres with diameters in the range of 200−220 nm were observed by SEM as shown in Figure 1c,d. Interestingly, the SEM images depicted in Figure 1c,d were obtained by using the samples without metallic coating. This fact implies that the nanospheres are highly conductive. We speculated that the nanospheres were polymerized products of 2-TAN because the polymerized products on Au nanoleaf surfaces were previously observed when $AuCl_4^-$ was reduced with 2-thiophenemethanol.[17]

To investigate the nature of nanospheres, we performed transmission electron microscopy (TEM) study. As depicted in Figure 2, the nanospheres were core/shell type of materials. The core Au NP was encapsulated with polythiophene conducting polymer shell. Interestingly, the layered structure of the polymer shell was clearly discernible (Figure 2b and the Supporting Information, Figure S2). The core/shell nanosphere with a metallic core surrounded by conducting polymer shells is a very interesting material. Although there are few examples of nanocomposites of Au with polyaniline conducting poly-

dx.doi.org/10.1021/am3019417 | ACS Appl. Mater. Interfaces 2012, 4, 6324−6331

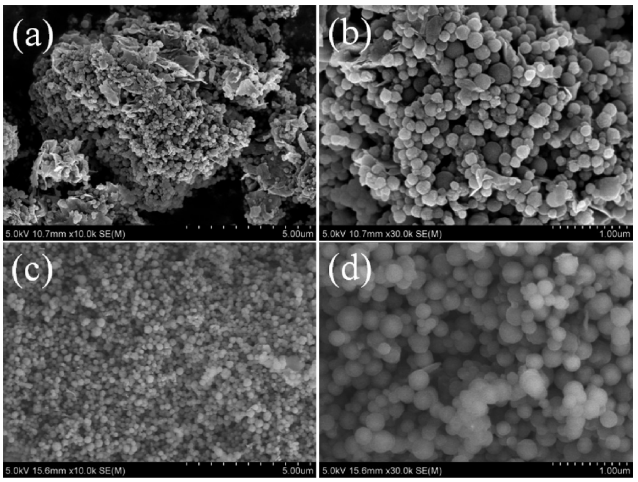

Figure 1. FE-SEM images of Au/Au@polythiophene core/shell nanospheres (a, b before) and (c, d) after an etching on different magnifications. Images shown in c and d were obtained by using samples without metallic coating. Conductive shell layer of core/shell nanospheres gave sufficient imaging capability without significant charging problems.

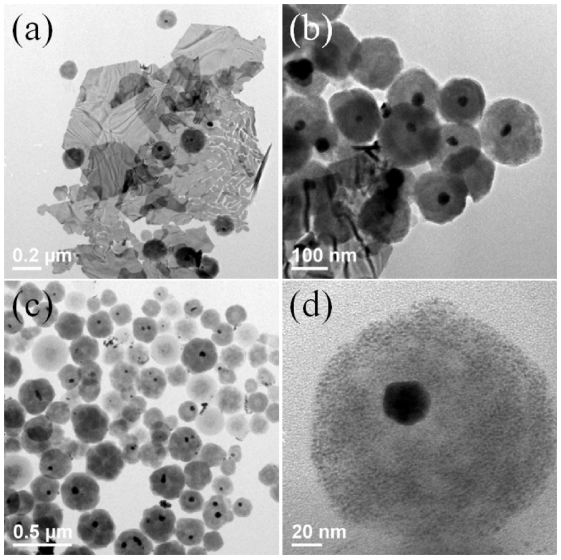

Figure 2. TEM images of the as-prepared Au materials (a, b) before and (c, d) after etching with KCN. Very tiny Au NPs uniformly embedded in conductive shells are clearly discernible in (d).

mer,[24,25] to the best of our knowledge, the Au/polythiophene core/shell hybrid nanostructure has not yet been reported.

Diameter distribution of the nanospheres was estimated based on the low magnification TEM images (Figure 2c). We found that a certain fraction of nanospheres did not contain a big Au NP core. Therefore, dimensional information of core/shell nanospheres and hollow nanospheres was collected separately (see the Supporting Information, Figure S3). Both core/shell nanospheres and hollow nanospheres showed relatively narrow particle size distributions ranging from 110 to 400 nm, with a maxima at a diameter range of 200−220 nm, suggesting overall dimensional uniformity of the nanospheres. Total numbers of measurements including hollow nanospheres were 726 and core/shell structured nanospheres were 440. This means that approximately 60 % of nanospheres contained a big Au NP core. On the basis of the high-resolution TEM (HR-TEM) image of an Au/polythiophene core/shell nanospheres, very tiny Au NPs uniformly embedded in the conductive shell were also observed (Figure 2d). The size of these tiny Au NPs in Figure 2d was in the range of 2 to 5 nm (see the Supporting Information, Figure S4). The uniform distribution of Au, S, and N elements in the core/shell nanospheres was revealed by SEM energy-dispersive X-ray spectroscopy (EDS) analysis as shown in Figure 3.

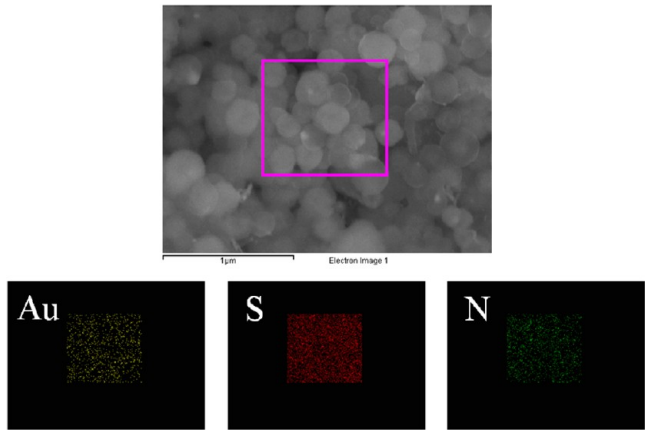

Figure 3. SEM EDS elemental mapping images of the Au/Au@polythiophene core/shell nanospheres by using samples without metallic coating.

The detailed elemental composition of the individual nanosphere was further investigated by high-angle annular dark-field scanning transmission electron microscopy (HAADF-STEM) line scanning analysis as depicted in panels a and b in Figure 4. The polymer shell also contained gold elements together with carbon elements. Hence, the shell was composed of evenly distributed very tiny Au NPs and polythiophene polymers. The detailed structure may be best described as Au/Au@polythiophene core/shell nanospheres. Even the hollow nanospheres were observed to possess very tiny Au NPs in the shell.

Formation kinetics of core/shell nanoshperes were probed by UV/Vis absorption spectroscopy during the formation periods as depicted in Figure S5 (see the Supporting Information). A typical SPR band of Au NPs appeared at 540−550 nm after 35 min and gradually increased after then (see the Supporting Information, Figure S5a).[26−28] After 120 min, however, the SPR band slowly decreased as the core/shell composites settled down from the solution. As shown in Figure S5a (see the Supporting Information), the reaction process was slow and it may be reasonable to speculate that the reduction process occurred at the interface of 2-TAN and water medium, which is also responsible for the formation of layered conducting polymer shell observed by HR-TEM. The formation of three different Au materials seemed to be a competitive process. Both hexagonal nanoplate and nanoleaf motifs had very similar structures to the previously reported nanoleaf formed by 2-thiophenemethanol. On the contrary, the formation mechanism of core/shell nanospheres was rather illusive. We propose that the initially formed big core Au NP by 2-TAN was surrounded by the growing 2-TAN polymer and tiny Au NPs were formed together in the shell. The core/shell nanospheres obtained after KCN etching exhibited two broad absorption bands centered at 361.5 nm and 564.9 nm because

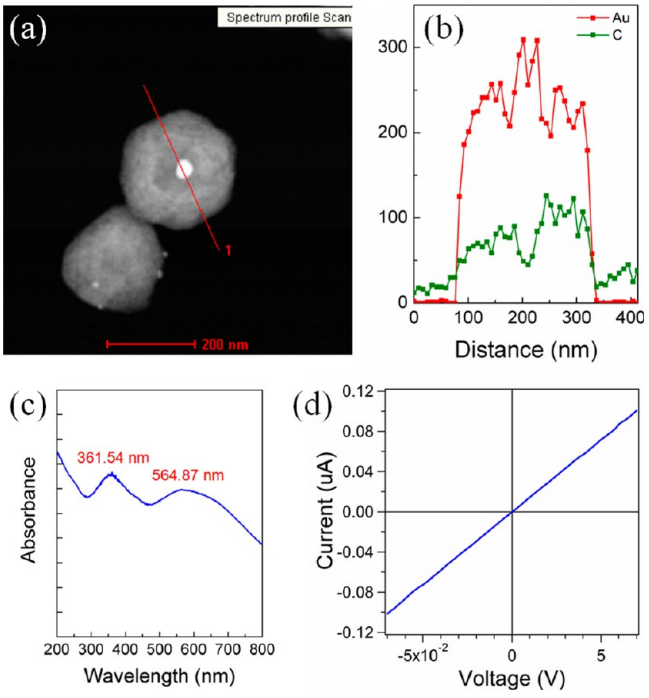

Figure 4. (a) HAADF-STEM image of an Au/Au@polythiophene core/shell nanosphere and (b) the corresponding EDS line scan profile. A big Au NP core is surrounded by the polythiophene shells embedding many tiny Au NPs. The neighboring nanosphere lacks the big Au core NP. (c) UV/vis absorption spectra of Au/Au@ polythiophene core/shell nanospheres after the KCN etching process and (d) the corresponding *I*–*V* plot obtained by using an IDA electrode.

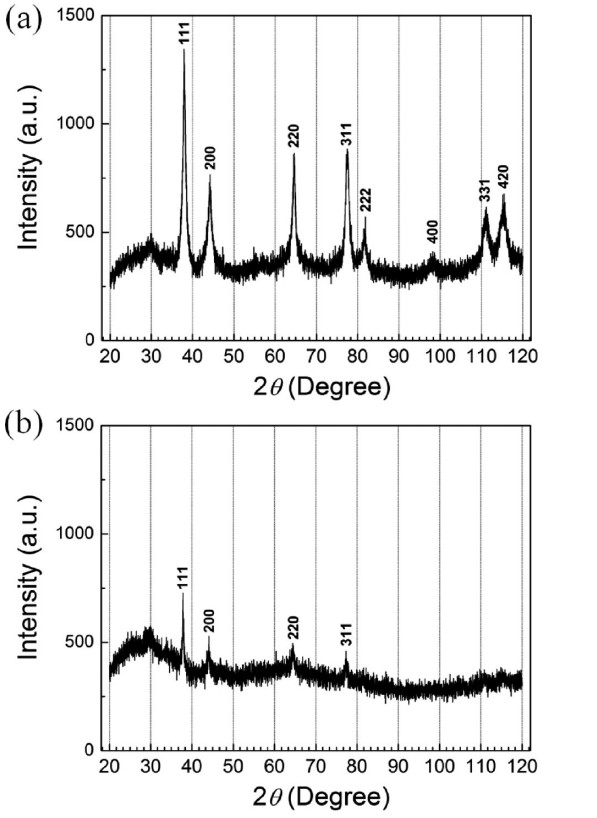

Figure 5. PXRD patterns of the samples obtained (a) before and (b) after KCN etching process showed typical fcc crystalline facets of Au. The four fcc peaks are still detectable after KCN etching process despite the much lower peak intensities.

of the thiophene-derived conducting polymer shell as shown in Figure 4c. These absorption bands were previously assigned to $\pi-\pi^*$ transition of a small π-conjugated system and a large π-conjugated system, respectively.[29] The existence of these bands demonstrates the core/shell structure with an Au NP core and the conductive polymer shell. The Au SPR band was completely buried in the absorption bands of polythiophene shells of the core/shell nanospheres.

The measurement of current–voltage relationship for core/shell nanospheres at varying potentials on an interdigitated electrode (IDA) was performed to investigate the electrical conductivity of the shell (see the Supporting Information, Figure S6). The ohmic behavior in Figure 4d indeed revealed the existence of conductive shell in Au core/shell nanospheres.

Metallic crystal lattices of core/shell Au nanospheres were confirmed by powder X-ray diffraction (PXRD) before and after the KCN etching process as depicted in Figure 5. Characteristic diffraction patterns of the face-centered cubic (fcc) lattice planes of metallic Au(0) were observed for both samples.[30] Comparing the PXRD patterns collected before and after the etching process, it can be evidently confirmed that virtually all the large hexagonal plates and nanoleaf structures were efficiently etched away. For example, the KCN-etched core/shell Au nanospheres exhibited relatively weak diffraction peaks at 37.82, 44.12, 64.40, and 77.34°, and these corresponded to (111), (200), (220), and (311) planes, respectively (Figure 5b, JCPDS No. 04-0784). Nevertheless, four typical fcc diffraction peaks were still identified after the etching process, which undoubtedly explained the existence of both cored Au NPs and shell-embedded tiny Au NPs.

The FT-IR spectra of neat 2-TAN and core/shell nanospheres after KCN etching were analyzed to identify the functionalities of the polymeric shell structure (Figure 6). A

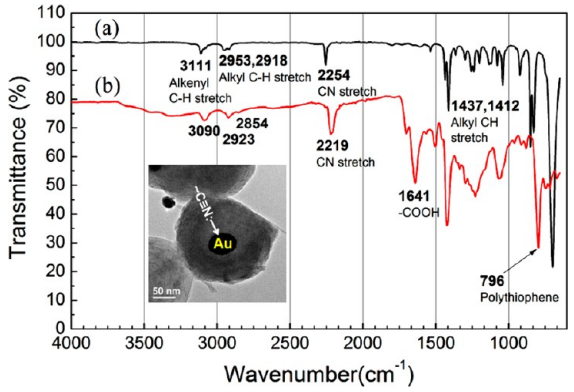

Figure 6. FT-IR spectra of (a) neat 2-TAN and (b) Au/Au@ polythiophene core/shell nanospheres. The Au-coordinated C≡N group is indicated (inset: TEM image).

strong absorption band at 796 cm^{-1} is the characteristic feature of thiophene-derived conducting polymer, which indicates successful polymerization of 2-TAN.[31] Stretching vibration for the C=C double bond of polythiophene usually appeared at 1641 cm^{-1} with a very weak intensity,[32] but in the spectrum of core/shell nanospheres, it showed a relatively strong absorption band at 1641 cm^{-1} possibly due to the carboxy functional group from the partial hydrolysis of the C≡N group in the acidic

dx.doi.org/10.1021/am3019417 | ACS Appl. Mater. Interfaces 2012, 4, 6324–6331

condition. A typical stretching band of ν(C≡N) for neat 2-TAN appeared at 2254 cm^{-1}. Notably, in the case of core/shell nanosphere, the C≡N bond showed a substantial red-shifted value of 35 cm^{-1} compared with that of the neat 2-TAN. It is well known that there are meaningful wavenumber shifts of the C≡N bond to either a higher or lower wavenumber upon coordination to transition metals.[33] In this point of view, we propose that there are considerable interactions of Au NPs with the surrounding C≡N bonds of the polythiophene shells. It is reasonable to attribute the different alignments of the C≡N groups in the surrounding polythiophene shell to the relative broadening of the stretching band of ν(C≡N) compared with that of the neat 2-TAN.

The formation of 2-TAN derivatives during the reaction was further monitored by electrospray ionization (ESI) mass spectrometry analysis of the reaction mixture (see the Supporting Information, Figure S7). Various species were derived from 2-TAN. The main species were 2,2′-bithiophene, 2-(5-(thiophen-2-yl)thiophen-2-yl)acetic acid, 2-(thiophen-2-yl)-*N*-((thiophen-2-yl)methyl)acetamide, 2-(5-(5-(5-(thiophen-2-yl)thiophen-2-yl)thiophen-2-yl)thiophen-2-yl)acetic acid, and other higher molecular weight derivatives, as well as a simple oxidized product, 2-thiophenecarboxaldehyde. Interestingly, some of the C≡N groups were indeed converted into carboxy groups under the acidic reaction condition. Therefore, several species had carboxy functionality as well as the C≡N group. On the basis of these results, it is very clear that polymerization is a key driving force for the reduction of Au precursor.

The elemental states of core/shell nanospheres were further investigated in detail using X-ray photoelectron spectroscopy (XPS) as shown in Figure 7. The spectrum was referenced to the binding energy of C 1s for the C−C bond as 284.8 eV.[34] The survey spectrum exhibited Au 4f, C 1s, N 1s, and S 2p peaks (Figure 7a). The high-resolution XPS spectrum displayed Au 4f doublet at 84.62 eV and 88.38 eV corresponding to metallic Au^0 $4f_{7/2}$ and $4f_{5/2}$ binding energies, respectively (Figure 7b). The binding energies of Au^0 were slightly higher than the reported values of bulk Au ($4f_{7/2}$ = 84.0 eV and $4f_{5/2}$ = 87.6 eV).[35] A very similar range of Au^0 $4f_{7/2}$ values was previously observed for supported Au NP catalysts such as Au/CeO_2 (84.5 eV) and Au/TiO_2 (84.4 eV).[36] Therefore, the surrounding environments of Au NPs were responsible for the increased binding energies of Au NPs. We may suggest that the coordination of the C≡N or COOH groups to Au NPs induced the change of binding energies of the Au surfaces. Interestingly, additional peaks attributable to Au^{3+} were observed at 87.06 and 90.57 eV with an area ratio of Au^0:Au^{3+} = 72%:28%. Thus, the Au species in core/shell nanospheres contained partially oxidized Au surfaces. The total content of Au element in the Au/Au@polythiophene core/shell nanospheres was 0.28 wt %. As shown in Figure 7a, the binding energies of N 1s peaks were observed at 399.19 and 401.06 eV[37] and the S 2p doublet appeared at 164.04 and 165.3 eV, and these values are in the usual level of binding energies found for S 2p in polythiophene.[38]

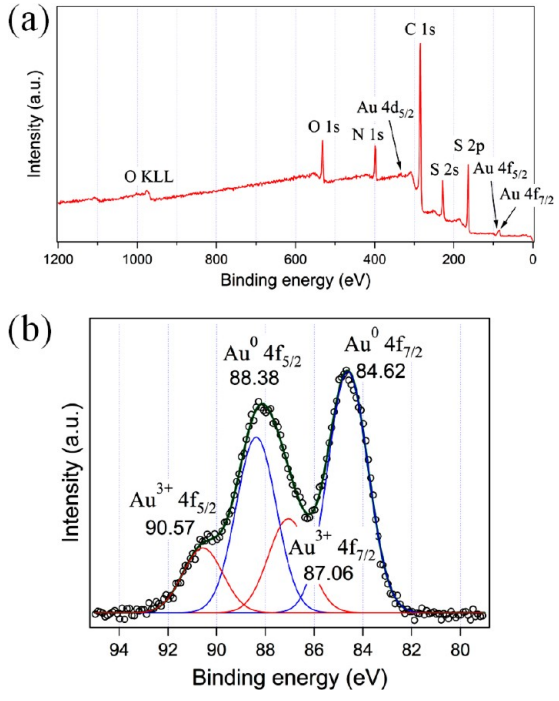

Figure 7. (a) XPS survey spectrum. (b) Deconvoluted Au 4f XPS spectrum for Au/Au@polythiophene core/shell nanospheres showing the state of Au element in the core/shell nanospheres.

Because the core/shell nanospheres contain Au NPs, they can be utilized as an active catalyst for the hydrogenation of nitroarene compounds.[39−41] To explore the ability of core/shell nanospheres as catalysts for the hydrogenation of various nitroarenes, 4-nitrophenol (4-NP), 4-nitrotoluene (4-NT) and nitrobenzene (NB) were employed as substrates in the presence of $NaBH_4$ as a hydrogen source. The results revealed that each reduction was performed in a well-defined manner and the reduction processes of nitroarene compounds could not proceed in the absence of core/shell nanospheres. The reduction kinetics of each nitroarene substrate was probed by UV/Vis absorption spectroscopy.

Typical evolutionary UV/Vis absorption spectra of the nitroarene reduction processes into aminoarene products are shown in Figure 8. For instance, in the case of 4-NP, the absorption band at 400 nm gradually decreased with time, and absorption at 300 nm concomitantly increased as 4-AP appeared with the isosbestic points at 319, 276, 248, and 222 nm, as shown in Figure 8a. Absorption maxima for the initial aqueous solution of 4-NP appeared at 317 nm, but its absorption band shifted to 400 nm after the addition of freshly prepared aqueous $NaBH_4$ solution since 4-nitrophenolate ion was formed. In the following reduction experiments, the characteristic absorption bands of 4-NT (284 nm) and NB (275 nm) were observed to diminish by lapse of time and the product bands of 4-AT (233 nm) and AB (231 nm) were accompanied and the isosbestic points were at 252 nm and 244 nm, respectively (Figure 8b,c). It is notable that the spectra have well-defined isosbestic points and this was an evident indication of sole product formation for nitroarene reduction without any byproduct generation.[42,43]

Even though it could be reasonably speculated that 4-NP was converted into 4-AP nearly a hundred percent based on the complete discoloration of the reaction mixture as a result of disappearance of the yellow-colored 4-NP substrate, it was difficult to derive the precise relationship between reactant concentration and the exact yield of 4-AP product as the absorbance at the final point of the reduction process was not zero due to the light scattering effect in the presence of core/shell nanosphere catalyst. Thus, we analyzed the reaction kinetics by comparing the linearly fitted regions between ln(C_t/

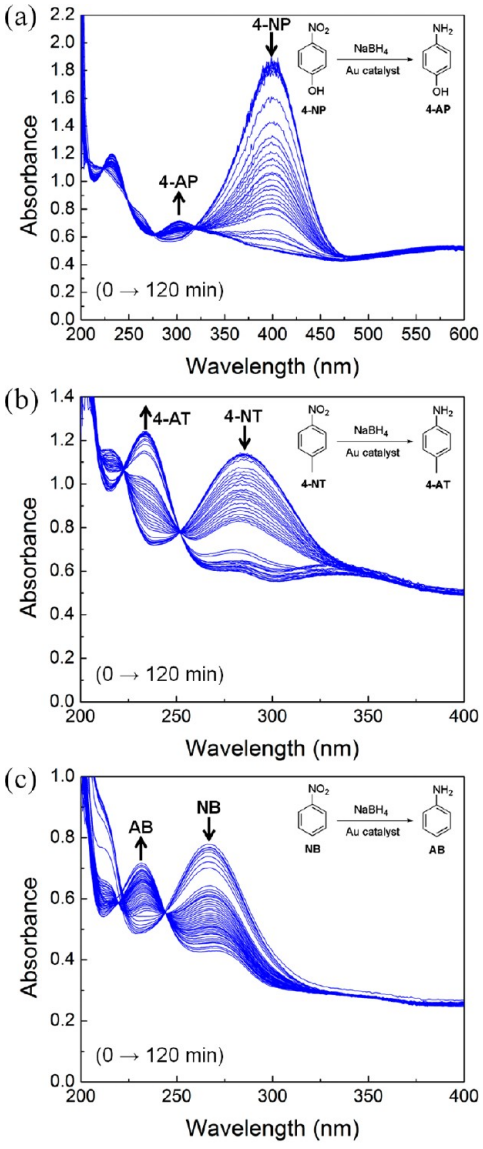

Figure 8. Time-dependent UV/Vis spectra for the reduction process of various nitroarene compounds with $NaBH_4$ and Au/Au@polythiophene core/shell nanosphere catalyst: (a) 4-nitrophenol, (b) 4-nitrotoluene, and (c) nitrobenzene. The absorbances of the reaction mixtures after the complete reaction of nitroarene substrates were not zero because the initial reaction mixture containing Au/Au@polythiophene core/shell nanospheres exhibited non-zero baseline in the UV/Vis absorption spectra.

C_0) and reaction time as shown in Figure 9. The reaction rate was shown to increase in the order of 4-NP > 4-NT > NB.

The respective pseudo-first-order reaction rate constants were calculated to be 0.039, 0.022, and 0.012 M min^{-1}. Although the water-soluble 4-NP was the most reactive than other hydrophobic substrates, both 4-NT and NB were also successfully converted into aminoarene products without much difficulty. Despite the induction periods for all substrates, the core/shell nanospheres were chemically accessible for the reactants and they provided suitable reaction environments for various substrates. We propose that both $NaBH_4$ and substrates need a certain time to diffuse into the shells of the core/shell nanosphere to react with catalytically active Au NPs embedded in the shells.

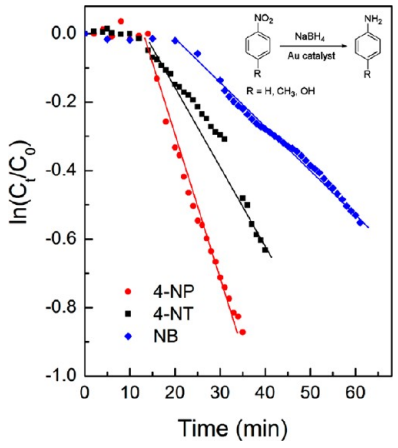

Figure 9. Time-dependent conversion plots for the reduction of nitroarenes by an Au/Au@polythiophene core/shell nanosphere catalyst with NaBH4. C_t indicates the concentrations of substrates at time t and C_0 is the initial concentrations of the substrates.

The Au/Au@polythiophene core/shell nanospheres exhibited two intense characteristic Raman scattering signals at 1509 and 1421 cm^{-1} upon 514 nm excitation as shown in Figure 10. These values slightly changed into 1505 and 1408

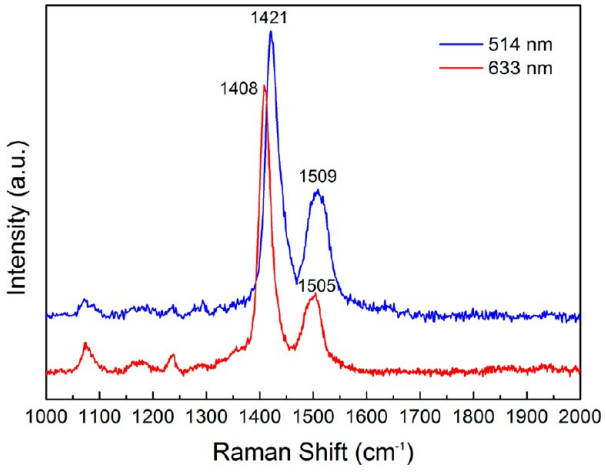

Figure 10. Raman spectra of Au/Au@polythiophene core/shell nanospheres with different excitation wavelengths.

cm^{-1} upon the variation of excitation wavelength of 633 nm. These two signals originated from the polythiophene shell of the core/shell nanospheres. Very similar Raman signals have been previously observed for Au nanoleaves in which polythiophenes from the 2-thiophenemethanol precursor stabilized the Au surfaces.[17] The peaks at 1509 and 1505 cm^{-1} are attributable to the C═C ring stretching mode of polythiophene. In contrast, the signals at 1421 and 1408 cm^{-1} were previously assigned as the quinoid forms of radical cations or dications of the oxidized polythiophene.[31]

It is noteworthy to mention that these intense characteristic Raman bands of the Au/Au@polythiophene core/shell nanospheres may be adequate for SERS applications because the functionalizable polythiophene shells embedding tiny Au NPs can behave as SERS tags without extra Raman reporter molecules.[44−46] The proximity of densely embedded Au NPs in the polythiophene shells may be responsible for the intense Raman signals due to the nanogap enhancement effect in

dx.doi.org/10.1021/am3019417 | ACS Appl. Mater. Interfaces 2012, 4, 6324−6331

SERS.[17,47−51] Furthermore, the core/shell nanospheres were thermally stable up to 200 °C based on thermogravimetric analysis (see the Supporting Information, Figure S8).

4. CONCLUSIONS

We successfully prepared a new type of nanoscale Au material, Au/Au@polythiophene core/shell nanospheres, by using 2-TAN as both reducing agent and shape control ligand. The core/shell nanospheres contained a big Au NP core surrounded by the polythiophene shells which also embedded many tiny Au NPs. The core/shell Au nanosphere turned out to be a very active hydrogenation catalyst for various hydrophilic and hydrophobic nitroarene substrates under mild conditions. The conductive shells of the core/shell nanospheres could be good supports for catalytically active Au NPs as demonstrated by the hydrogenation of both hydrophilic and hydrophobic substrates. Interestingly, there were short induction periods for all substrates. The core/shell nanosphere also exhibited very strong Raman absorption signals due to the polythiophene shells with tiny Au NPs. We are currently investigating the effect of SERS on the core/shell nanospheres.

■ ASSOCIATED CONTENT

Ⓢ Supporting Information

Cyclic voltammogram of 2-TAN, HR-TEM images of the as-prepared Au/polythiophene materials, diameter distributions of core/shell nanospheres, diameter distribution Au NPs, time-dependent UV/vis absorption spectra, *I*−*V* measurement setup, ESI mass spectrum, and TG profile. This material is available free of charge via the Internet at http://pubs.acs.org/.

■ AUTHOR INFORMATION

Corresponding Author

*E-mail: shuh@hufs.ac.kr.

Author Contributions

The manuscript was written through contributions of all authors.

Notes

The authors declare no competing financial interest.

■ ACKNOWLEDGMENTS

This work was supported by Hankuk University of Foreign Studies Research Fund of 2012.

■ ABBREVIATIONS

NP, nanoparticle; 2-TAN, 2-thiopheneacetonitrile; FT-IR, Fourier transform-infrared; TEM, transmission electron microscopy; SEM, scanning electron microscopy; EDS, energy dispersive X-ray spectroscopy; PXRD, powder X-ray diffraction; XPS, X-ray photoelectron spectroscopy; SERS, surface-enhanced Raman scattering; TG, thermogravimetric

■ REFERENCES

(1) Storhoff, J. J.; Mirkin, C. A. *Chem. Rev.* **1999**, *99*, 1849−1862.
(2) Pérez-Juste, J.; Pastoriza-Santos, I.; Liz-Marzán, L. M.; Mulvaney, P. *Coord. Chem. Rev.* **2005**, *249*, 1870−1901.
(3) Kanayama, N.; Takarada, T.; Maeda, M. *Chem. Commun.* **2011**, *47*, 2077−2079.
(4) Su, X.; Kanjanawarut, R. *ACS Nano* **2009**, *3*, 2751−2759.
(5) Liu, R.; Liew, R.; Zhou, J.; Xing, B. *Angew. Chem., Int. Ed.* **2007**, *46*, 8799−8803.
(6) Murphy, C. J.; Sau, T. K.; Gole, A. M.; Orendorff, C. J.; Gao, J.; Gou, L.; Hunyadi, S. E.; Li, T. *J. Phys. Chem. B* **2005**, *109*, 13857−13870.
(7) Yin, J.; Wu, T.; Song, J.; Zhang, Q.; Liu, S.; Xu, R.; Duan, H. *Chem. Mater.* **2011**, *23*, 4756−4764.
(8) Xu, L.; Kuang, H.; Xu, C.; Ma, W.; Wang, L.; Kotov, N. A. *J. Am. Chem. Soc.* **2012**, *134*, 1699−1709.
(9) Patra, C. R.; Bhattacharyaa, R.; Mukherjee, P. *J. Mater. Chem.* **2010**, *20*, 547−554.
(10) Rosi, N. L.; Giljohann, D. A.; Thaxton, C. S.; Lytton-Jean, A. K. R.; Han, M. S.; Mirkin, C. A. *Science* **2006**, *312*, 1027−1030.
(11) Haruta, M.; Yamada, N.; Kobayashi, T.; Iijima, S. *J. Catal.* **1989**, *115*, 301−309.
(12) Chen, M.; Goodman, D. W. *Acc. Chem. Res.* **2006**, *39*, 739−746.
(13) Ma, Z.; Dai, S. *Nano Res.* **2011**, *4*, 3−32.
(14) Xu, L.; Ren, Y.; Wu, H.; Liu, Y.; Wang, Z.; Zhang, Y.; Xu, J.; Peng, H.; Wu, P. *J. Mater. Chem.* **2011**, *21*, 10852−10858.
(15) Lee, J.; Park, J. C.; Song, H. *Adv. Mater.* **2008**, *20*, 1523−1528.
(16) Liu, R.; Mahurin, S. M.; Li, C.; Unocic, R. R.; Idrobo, J. C.; Gao, H.; Pennycook, S. J.; Dai, S. *Angew. Chem., Int. Ed.* **2011**, *50*, 6799−6802.
(17) Hong, J.-H.; Hwang, Y.-K.; Hong, J.-Y.; Kim, H.-J.; Kim, S.-J.; Won, Y. S.; Huh, S. *Chem. Commun.* **2011**, *47*, 6963−6965.
(18) Jin, R.; Cao, Y. C.; Hao, E.; Métraux, G. S.; Schatz, G. C.; Mirkin, C. A. *Nature* **2003**, *425*, 487−490.
(19) Xia, Y.; Xiong, Y.; Lim, B.; Skrabalak, S. E. *Angew. Chem., Int. Ed.* **2009**, *48*, 60−103.
(20) Goebl, J.; Zhang, Q.; He, L.; Yin, Y. *Angew. Chem., Int. Ed.* **2012**, *51*, 552−555.
(21) Xue, C.; Chen, X.; Hurst, S. J.; Mirkin, C. A. *Adv. Mater.* **2007**, *19*, 4071−4074.
(22) Shankar, S. S.; Rai, A.; Ankamwar, B.; Singh, A.; Ahmad, A.; Sastry, M. *Nat. Mater.* **2004**, *3*, 482−488.
(23) Shin, H. S.; Lim, H.; Song, H. J.; Shin, H.-J.; Park, S.-M.; Choi, H. C. *J. Mater. Chem.* **2010**, *20*, 7183−7188.
(24) Zhang, B.; Zhao, B.; Huang, S.; Zhang, R.; Xu, P.; Wang, H.-L. *CrystEngComm* **2012**, *14*, 1542−1544.
(25) Berzina, T.; Gorshkov, K.; Pucci, A.; Ruggerid, G.; Erokhin, V. *RSC Adv.* **2011**, *1*, 1537−1541.
(26) Li, H.; Jo, J.; Wang, J.; Zhang, L.; Kim, I. *Cryst. Growth Des.* **2010**, *10*, 5319−5326.
(27) Sun, X.; Dong, S.; Wang, E. *Angew. Chem., Int. Ed.* **2004**, *43*, 6360−6363.
(28) Zhu, T.; Vasilev, K.; Kreiter, M.; Mittler, S.; Knoll, W. *Langmuir* **2003**, *19*, 9518−9525.
(29) Li, X.-G.; Li, J.; Huang, M.-R. *Chem.—Eur. J.* **2009**, *15*, 6446−6455.
(30) Xu, J.; Li, S.; Weng, J.; Wang, X.; Zhou, Z.; Yang, K.; Liu, M.; Chen, X.; Cui, Q.; Cao, M.; Zhang, Q. *Adv. Funct. Mater.* **2008**, *18*, 277−284.
(31) Peng, H.; Zhang, L.; Spires, J.; Soeller, C.; Travas-Sejdic, J. *Polymer* **2007**, *48*, 3413−3419.
(32) Lim, J.-S.; Lee, K.; Choi, J.-N.; Hwang, Y.-K.; Yun, M.-Y.; Kim, H.-J.; Won, Y. S.; Kim, S.-J.; Kwon, H.; Huh, S. *Nanotechnolgy* **2012**, *23*, 085101.
(33) Huh, S.; Suh, M.-J.; Vien, V.; Kim, Y.; Hwang, S.-J.; Kim, S.-J. *Small* **2009**, *5*, 1123−1127.
(34) Pijpers, A. P.; Meier, R. J. *Chem. Soc. Rev.* **1999**, *28*, 233−238.
(35) Wang, Z.; Zhang, Q.; Kuehner, D.; Ivaska, A.; Niu, L. *Green Chem.* **2008**, *10*, 907−909.
(36) Casaletto, M. P.; Longo, A.; Martorana, A.; Prestianni, A.; Venezia, A. M. *Surf. Interface Anal.* **2006**, *38*, 215−218.
(37) Sun, L.; Wang, L.; Tian, C.; Tan, T.; Xie, Y.; Shi, K.; Li, M.; Fu, H. *RSC Adv.* **2012**, *2*, 4498−4506.
(38) Natarajan, S.; Kim, S. H. *Chem. Commun.* **2006**, 729−731.
(39) Wu, S.; Dzubiella, J.; Kaiser, J.; Drechsler, M.; Guo, X.; Ballauff, M.; Lu, Y. *Angew. Chem., Int. Ed.* **2012**, *51*, 2229−2233.
(40) Wei, J.; Wang, H.; Deng, Y.; Sun, Z.; Shi, L.; Tu, B.; Luqman, M.; Zhao, D. *J. Am. Chem. Soc.* **2011**, *133*, 20369−20377.

(41) Liu, B.; Zhang, W.; Feng, H.; Yang, X. *Chem. Commun.* **2011**, *47*, 11727−11729.
(42) Dong, F.; Guo, W.; Park, S.-K.; Ha, C.-S. *Chem. Commun.* **2012**, *48*, 1108−1110.
(43) Deng, Y.; Cai, Y.; Sun, Z.; Liu, J.; Liu, C.; Wei, J.; Li, W.; Wang, Y.; Zhao, D. *J. Am. Chem. Soc.* **2010**, *132*, 8466−8473.
(44) Liu, X.; Knauer, M.; Ivleva, N. P.; Niessner, R.; Haisch, C. *Anal. Chem.* **2010**, *82*, 441−446.
(45) Samanta, A.; Maiti, K. K.; Soh, K.-S.; Liao, X.; Vendrell, M.; Dinish, U. S.; Yun, S.-W.; Bhuvaneswari, R.; Kim, H.; Rautela, S.; Chung, J.; Olivo, M.; Chang, Y.-T. *Angew. Chem., Int. Ed.* **2011**, *50*, 6089−6092.
(46) Kairdolf, B. A.; Nie, S. *J. Am. Chem. Soc.* **2011**, *133*, 7268−7271.
(47) Lim, D.-K.; Jeon, K.-S.; Kim, H. M.; Nam, J.-M.; Suh, Y. D. *Nat. Mater.* **2010**, *9*, 60−67.
(48) Haran, G. *Acc. Chem. Res.* **2010**, *43*, 1135−1143.
(49) Jin, R. *Angew. Chem., Int. Ed.* **2010**, *49*, 2826−2829.
(50) Mulvihill, M.; Tao, A.; Benjauthrit, K.; Arnold, J.; Yang, P. *Angew. Chem., Int. Ed.* **2008**, *47*, 6456−6460.
(51) Lee, S. Y.; Hung, L.; Lang, G. S.; Cornett, J. E.; Mayergoyz, I. D.; Rabin, O. *ACS Nano* **2010**, *4*, 5763−5772.